Chem Biol Drug Des 2016; **87:** 112–120

Research Article

Site-directed Mutagenesis of Key Residues Unveiled a Novel Allosteric Site on Human Adenosine Kinase for Pyrrolobenzoxa(thia)zepinone Non-Nucleoside Inhibitors

Lida Savi[1], Margherita Brindisi[2,3], Gloria Alfano[2,3], Stefania Butini[2,3,*], Valeria La Pietra[3,4], Ettore Novellino[3,4], Luciana Marinelli[3,4,*], Andrea Lossani[1], Federico Focher[1,*], Caterina Cavella[2,3], Giuseppe Campiani[2,3] and Sandra Gemma[2,3]

[1]Istituto di Genetica Molecolare, CNR, Via Abbiategrasso 207, 27100 Pavia, Italy
[2]Dipartimento di Biotecnologie, Chimica e Farmacia, University of Siena, via Aldo Moro 2, 53100 Siena, Italy
[3]European Research Centre for Drug Discovery and Development (NatSynDrugs), University of Siena, via Aldo Moro 2, 53100 Siena, Italy
[4]Dipartimento di Farmacia, Università di Napoli Federico II, via D. Montesano 49, 80131 Napoli, Italy
**Corresponding authors: Stefania Butini, butini3@unisi.it; Luciana Marinelli, luciana.marinelli@unina.it; Federico Focher, focher@igm.cnr.it*
L.S. and M.B. equally contributed to this work.

Most nucleoside kinases, besides the catalytic domain, feature an allosteric domain which modulates their activity. Generally, non-substrate analogs, interacting with allosteric sites, represent a major opportunity for developing more selective and safer therapeutics. We recently developed a series of non-nucleoside non-competitive inhibitors of human adenosine kinase (*h*AK), based on a pyrrolobenzoxa(thia) zepinone scaffold. Based on computational analysis, we hypothesized the existence of a novel allosteric site on *h*AK, topographically distinct from the catalytic site. In this study, we have adopted a multidisciplinary approach including molecular modeling, biochemical studies, and site-directed mutagenesis to validate our hypothesis. Based on a three-dimensional model of interaction between *h*AK and our molecules, we designed, cloned, and expressed specific, single and double point mutants of *h*AK (Q74A, Q78A, H107A, K341A, F338A, and Q74A-F338A). Kinetic characterization of recombinant enzymes indicated that these mutations did not affect enzyme functioning; conversely, mutated enzymes are endowed of reduced susceptibility to our non-nucleoside inhibitors, while maintaining comparable affinity for nucleoside inhibitors to the wild-type enzyme. This study represents the first characterization and validation of a novel allosteric site in *h*AK and may pave the way to the development of novel selective and potent non-nucleoside inhibitors of *h*AK endowed with therapeutic potential.

Key words: adenosine kinase, Ala-scan mutagenesis, allosteric binding site, allosteric inhibitors, drug discovery, non-nucleoside human AK inhibitors, small molecule

Abbreviations: 5-ITU, 5-iodo-7-β-D-ribofuranosyl-7*H*-pyrrolo[2,3-*d*]pyrimidin-4-amine; Ado, adenosine; CNS, central nervous system; *h*AK, human AK; Hcy, homocysteine; IPTG, isopropylthio-β-D-galactoside; KHK, ketohexokinase; NN*h*AKIs, non-nucleoside *h*AK inhibitors; PNS, peripheral nervous system; RK, ribokinase; SAH, *S*-adenosylhomocysteine; wt, wild type.

Received 24 April 2015, revised 24 July 2015 and accepted for publication 27 July 2015

Adenosine kinase (AK; EC.2.7.1.20) plays an important role in regulating the intracellular as well as extracellular concentrations of adenosine (Ado) (1,2), a nucleoside which exerts a broad range of physiological responses via interaction with Ado receptors. Due to its diverse physiological actions, abnormal Ado concentrations are involved in several diseases, especially in those affecting central and peripheral nervous systems (CNS, PNS), where the fine-tuning of Ado concentration appears to hold a particular physiological relevance (3). *Human* AK (*h*AK) activity was also found to play a role in the regulation of cardiac hypertrophy (4) and diabetes (5). In view of the enormous pharmacological potential of Ado, there has been much interest in studying role and modulation of AK over the years (6). Recently, it has been demonstrated that *h*AK activity could also play an important role in the epigenetic control of nucleic acids (7,8). Cytidine methylation is strategic for gene expression and regulation and requires the donation of a methyl group from S-adenosylmethionine, a process that is catalyzed by DNA methyltransferases. The resulting product, S-adenosylhomocysteine (SAH), is then converted into Ado and homocysteine (Hcy) by SAH hydrolase (7). Critically, the equilibrium constant of the SAH hydrolase enzyme lies in the direction of SAH formation (9); therefore, the reaction will only proceed when Ado and Hcy are constantly removed (9,10). In the

 doi: 10.1111/cbdd.12630

adult brain, removal of Ado occurs largely via the astrocytic *h*AK (2,3). If this *h*AK-mediated metabolic clearance of Ado is impaired, SAH levels rise (10) and inhibit methyltransferases by product inhibition (11). Thus, intracellular concentration of Ado could be crucial to control DNA methylation and gene expression (7). Accordingly, it has been observed that Ado induces hypomethylation of DNA via biochemical interference with the transmethylation pathway (7). The Boison's group effectively treated epileptogenesis in multiple seizure models by delivering Ado into the brain. They observed that global DNA methylation was significantly reduced (by 51%) in the hippocampus of treated versus control animals. It was proved in rats that temporal lobe epilepsy correlates with an increase in hippocampal DNA methylation, DNA methyltransferase activity, disruption of Ado homeostasis, and spontaneous recurrent seizures. Thus, pathological changes in DNA methylation patterns may trigger epilepsy and reversal of these epigenetic changes with Ado therapy may halt disease progression. Moreover, modulation of the 'adenosinergic system' may be relevant in therapy of other CNS disorders such as schizophrenia, Alzheimer's disease, Huntington's disease, amyotrophic lateral sclerosis, and multiple sclerosis (6). However, the systemic administration of Ado (unless directly injected in brain) has proved inefficient because of its short half-life in physiological fluids, poor bioavailability, rapid uptake by erythrocytes, lack of specificity, and long-term cytotoxic effects (3). At the same time, Ado receptor agonists may lead to unfavorable side-effect caused by the activation of Ado receptors in non-target tissues. Accordingly, the inhibition of Ado-metabolizing enzymes, such as *h*AK, represents a valuable alternative to elevate the Ado levels in specific brain areas.

*h*AK is an evolutionarily ancient and highly conserved enzyme, which is directly related to bacterial ribokinases and fructokinases (12,13). *h*AK catalyzes the phosphorylation of Ado to AMP, using ATP as a phosphate donor. The *h*AK structure in complex with two Ado molecules has been solved by Mathews and colleagues (14). The human enzyme works as a monomer (13) and is composed by twelve α-helices and fourteen β-sheets and is featured by (i) a catalytic Ado binding site, (ii) a regulatory Ado binding site, (iii) an ATP binding site, and (iv) three Mg^{2+} binding sites, one of which essential for the catalytic reaction (15).

Due to their relevant role in cell metabolism, Ado and ATP are molecules which interact with several enzymes. Thus, synthetic inhibitors that interact with the active site of enzymes metabolizing Ado or ATP, although potent, are generally poorly selective and therefore toxic. Their low specificity could be expected even if Ado- or ATP-metabolizing enzymes do not share amino acid sequences homology in their catalytic pockets; structural homology could be enough.

Aware of this issue, we recently developed a novel class of non-toxic non-nucleoside and non-competitive *h*AK inhibitors (NN*h*AKIs) able to inhibit the enzyme activity in the micromolar range (16). These compounds are characterized by a unique molecular scaffold, and interestingly they showed a different mechanism of action compared to known NN*h*AKIs. The kinetic behavior of our pyrrolobenzoxa(thia)zepines suggested the existence of an allosteric site, topographically distinct from the alkynylpyrimidine binding site. Based on these data, a computational analysis, using *h*AK in different conformations (open and closed), was performed for identifying the NN*h*AKIs' allosteric binding site. This original analysis revealed the presence of a shallow pocket located between the helices α3, α4, and the carboxylic tail which is upon the Ado and ATP binding sites (16). Intriguingly, this pocket was clearly detectable only in the closed conformation of *h*AK, while it was only partially evident in the open conformation due to the shift of the β4-sheet (16).

Starting from the hypothesized binding site and our ligand binding mode (Figure 1), we report herein an alanine scanning mutagenesis and a biochemical study to support our original hypothesis and to confirm the presence of an allosteric binding site in *h*AK for NN*h*AKIs. This study deals with the cloning, expression, and biochemical characterization of several single and double *h*AK mutants, the stereoselective synthesis of the most potent NN*h*AKIs, the binding experiments against wild-type (wt) and all mutants. This approach led to the validation of a novel allosteric binding site on *h*AK, the exploitation of which may lead to new avenues for the discovery of selective and safe therapeutics.

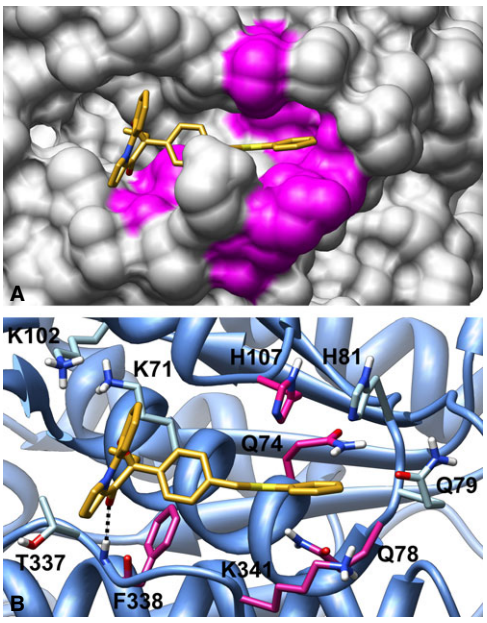

Figure 1: Binding pose of **NSD438** in the allosteric site of *h*AK showed as cornflower cartoon (panel A). Interacting residues are shown as sticks and colored by atom type, while the H-bond is represented by a black dashed line (panel B). Residues are labeled according to PDB numbering.

Methods and Materials

Chemistry

Starting materials and solvents were purchased from commercial suppliers and used without further purification. Reaction progress was monitored by TLC using silica gel 60 F254 (0.040–0.063 μm) with detection by UV. Silica gel 60 (0.040–0.063 μm) was used for column chromatography. Yields refer to purified materials and are not optimized. ^{1}H NMR and ^{13}C NMR spectra were recorded on a Varian 300 MHz or a Bruker 400 MHz spectrometer using the residual signal of the deuterated solvent as internal standard. Splitting patterns are described as singlet (s), doublet (d), triplet (t), quartet (q), and broad (br); chemical shifts (δ) are given in ppm and coupling constants (J) in hertz (Hz). ESI-MS spectra were performed by an Agilent 1100 Series LC/MSD spectrometer. Optical rotation values were measured at room temperature using a Perkin–Elmer model 343 polarimeter operating at 589 nm, corresponding to the sodium D line or a Jasco P-2000 polarimeter operating at 436 nm. All moisture-sensitive reactions were performed under argon atmosphere using oven-dried glassware and anhydrous solvents. Elemental analyses were performed in a Perkin–Elmer 240C elemental analyzer. For (*R*)- and (*S*)-**NSD438**, they were in full agreement with the values found for racemic **NSD438** (16) and the results were within ± 0.4% of the theoretical values. The synthesis of (*R*)- and (*S*)-**NSD438** is reported in Scheme 1. Compounds **14**–**19** were synthesized as previously reported by us (16). Synthetic procedures and characterization data for the new compounds are given in the Supporting Information (Appendix S1).

Biology

For biological tests analytical grade reagents were exclusively used. Bacterial media components were from Difco. Ni-NTA Superflow resin was from Qiagen. Restriction and modification enzymes were from Promega, Sigma, or Roche Molecular Biochemicals. Vectors were from Invitrogen. Isopropylthio-β-D-galactoside (IPTG) was from Sigma. [2,8-^{3}H]-Ado, 29.1 Ci/mmol, was from Hartmann Analytic.

Site-directed mutagenesis of recombinant hAK

Human AK mutants were obtained through PCR mutagenesis (17) using the wt-*h*AK gene (1070 bp), inserted into pTrcHisA vector (16), and the primers reported in Table S1.

For single-site and double-site mutations, the PCR (50 μL) contained 50 ng of DNA template (pTrcHisA-wt-*h*AK), 0.1 μM primer pair, 250 μM dNTPs, and 3U of PfuUltra High-fidelity DNA polymerase (Agilent Technologies©). The PCR cycles were initiated at 95 °C for 5 min, followed by 12 amplifications (95 °C for 1 min, 62 °C for 1 min, and 68 °C for 12 min). The last step was performed at 68 °C for 1 h. To eliminate parental wt DNA, the PCR products were treated with 10 U of *DpnI* at 37 °C for 3 h and then 10 μL of digestion product was analyzed by agarose gel electrophoresis. The full-length plasmid was quantified using DNA Molecular Marker III as reference (0.21–21.2 kbp; Roche Applied Science). Then, 1 ng of mutated DNA was use to transform *E. coli* (DH5α strain) TSS chemically competent cells (18). All mutants were sequenced by Bmr Genomics (Padova, Italy) to confirm the presence of the desired mutation and the absence of undesired mutations.

Expression and purification of recombinant wt-hAK and hAK mutants

Wild-type and mutant proteins were purified from *E. coli* crude extract in a single chromatographic step using Ni-NTA Superflow column (Qiagen). Briefly, a fresh overnight saturated culture of bacteria was diluted 1:100 in 1 L of 2 × YT medium containing ampicillin (75 μg/mL) and incubated at 37 °C with shaking. At OD_{600}, IPTG was added to a final concentration of 0.4 mM, and culture was incubated for 2 h at 25 °C.

The bacterial cell pellet was resuspended in four volumes of lysis buffer (50 mM sodium phosphate, pH 8.0, 300 mM NaCl, 10 mM imidazole). Lysozyme 1 mg/mL and PMSF 1 mM were also added, and the mixture was incubated on ice for 30 min. Cells were sonicated (6 × 10 seconds, 85 dCy) and homogenized. Then, the lysate was centrifuged at 20 000 *g* for 30 min at 4 °C. The supernatant was loaded into Ni-NTA Superflow column (1 mL) previously equilibrated in lysis buffer. The column was then washed with 10 mL of lysis buffer, followed by 10 mL of wash buffer containing 50 mM sodium phosphate, pH 8.0, 300 mM NaCl, 20 mM imidazole. The protein was then eluted by a gradient from 20 to 250 mM imidazole in 50 mM sodium phosphate buffer, pH 8.0, and 300 mM NaCl. The *h*AK-rich fractions were pooled and dialyzed against 50 mM Tris–HCl pH 7.5 containing 1 mM 1,4-dithiothreitol (DTT) and 20% glycerol and then frozen in liquid nitrogen until used.

Biochemical characterization of recombinant wt-hAK and hAK mutants

Wild-type and mutated *h*AK were assayed with a radiochemical method which measures the formation of [^{3}H]-AMP from [^{3}H]-Ado. The enzyme was incubated at 37 °C in 15 μL of a mixture containing 64 mM Tris–HCl (pH 7.5), 40 mM KCl, 0.1 mM $MgCl_2$, 0.1 mM ATP, and 1 μM [2,8-^{3}H]-Ado (29.1 Ci/mmol, 750 cpm/pmol; Hartmann Analytic). The reaction was terminated by spotting 10 μL of the incubated mixture on DEAE 96-square glass fiber filter (DEAE Filtermat; Wallac). The filter was rinsed three times in 1 mM ammonium formate, pH 3.6, to remove unconverted nucleoside, and finally in ethanol. The filter was dried and melt on scintillator sheets (MeltiLex A; Perkin Elmer), and labeled-AMP trapped on filter was quantified by Microbeta Trilux (Perkin Elmer) luminometer, according to the manufacturer's protocol.

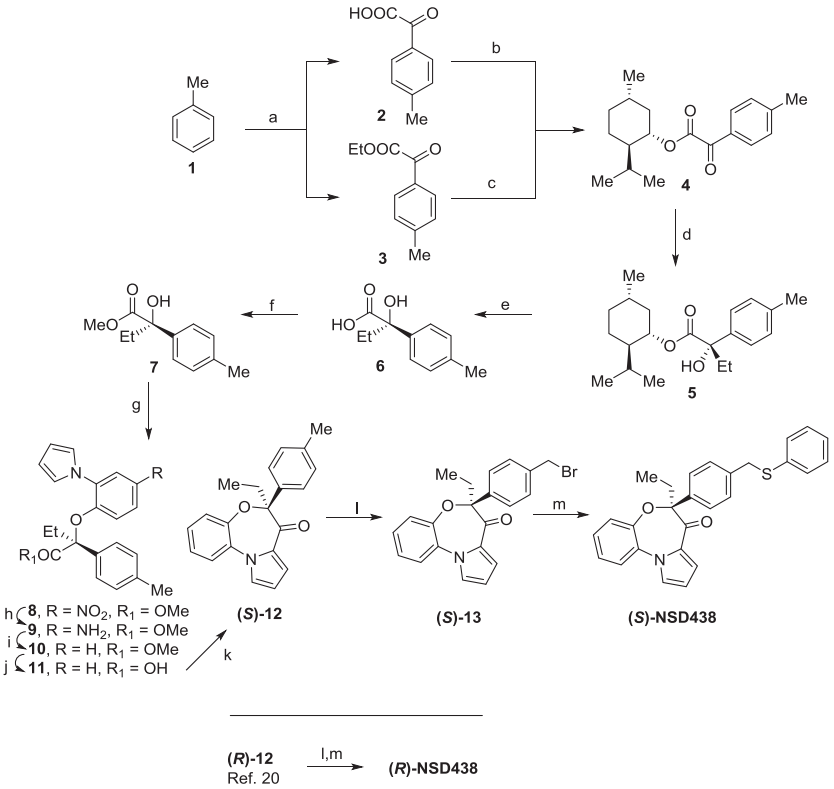

Scheme 1: Stereoselective synthesis of compounds (*S*)- and (*R*)-NSD438. Reagents and conditions: (a) $AlCl_3$, ClCOCOOEt, 1,2-DCE, from 0 to 30 °C, 3 h; (b) (1*S*,2*R*,5*S*)-(+)-menthol, *p*-TsOH, dry toluene, 120 °C, 12 h; (c) (1*S*,2*R*,5*S*)-(+)-menthol, $Ti[OCH(CH_3)_2]_4$, dry toluene, 100 °C, 12 h; (d) EtMgBr, $ZnCl_2$, 5 h, from 0 °C (2 h) to −78 °C (3 h), then to rt (1 h); (e) KOH, MeOH/H_2O 1:1, reflux, 24 h; (f) MeI, K_2CO_3, dry DMF, rt, 5 h; (g) 1-(2-fluoro-5-nitrophenyl)-1*H*-pyrrole, NaH, dry THF, rt, 12 h; (h) $SnCl_2$, EtOH, 80 °C, 5 h; (i) $NaNO_2$, $NaHSO_3$, AcOH, EtOH, rt, 3 h; (j) 15% NaOH, EtOH/THF, rt, 2 h; (k) PCl_5, dry CH_2Cl_2, 40 °C, 12 h; (l) NBS, AIBN, CCl_4, 80 °C, 7 h; (m) NaH, thiophenol, dry THF, rt, 10 h.

Inhibition assay of recombinant wt-hAK and hAK mutants

In inhibition studies, increasing concentrations of each compound were tested in duplicate in two independent assays, as described above. Stock solutions of compound, in 100% DMSO, were diluted in water to a final DMSO concentration of 1%. Controls without inhibitor were also incubated in the presence of 1% DMSO. Reference inhibitor used 5-iodo-7-*β*-D-ribofuranosyl-7H-pyrrolo[2,3-*d*]pyrimidin-4-amine (5-ITU) purchased from Tocris Bioscience (19).

Molecular modeling

Molecular docking

The docking was performed with the aid of GLIDE software where the 'write per-residue interaction score' feature is implementeda. The **NSD438** inhibitor structures were first generated through the Dundee PRODRG2 server. Then, geometry optimized ligands were prepared using LIG-PREP 2.3 as implemented in MAESTRO. The 1BX4 closed conformation of the *h*AK protein was prepared through the Protein Preparation Wizard of the graphical user interface Maestro and the OPLS-2001 force field. Water molecules were removed. Hydrogen atoms were added, and minimization was performed until the rmsd of all heavy atoms was within 0.3 Å of the crystallographically determined positions. The binding pocket was identified by placing a 15 Å cube centered on the F338 mass center. Molecular docking calculations were performed with the aid of GLIDE 5.5 in standard precision (SP) mode.

Multiple sequence alignment

Multiple sequence alignment of AK with related proteins, ribokinase (RK) and ketohexokinase (KHK), was performed using CLUSTALW2 (http://www.ebi.ac.uk/Tools/msa/clustalw2). Although we were interested only on human proteins, also sequences from rat and mouse were included to achieve a more reliable alignment.

Results and Discussion

hAK mutants and selection of NNhAKIs

Our early computational analysis of *h*AK allowed us to raise the hypothesis on the existence of an unprecedentedly described allosteric site on the surface of the closed conformation of *h*AK (16).

The computational evidence of an allosteric mode of action was further strengthened by the fact that the inhibitory potency of **NSD438** was unaffected by increasing concentrations of the AK substrates Ado or ATP, indicat-

ing a non-competitive mode of inhibition (16). In the newly identified pocket, our lead **NSD438** was found, thorough docking studies, to lie on α3 helix sandwiched between helix α4 and the long carboxylic tail. Analysis of the key interactions between **NSD438** and *h*AK highlighted F338 as key residue in the interaction with the ligand, as an H-bond and a π–π interaction was found with **NSD438** (16) (Figure 1).

On the carboxylic tail, two residues (F338 and K341) were found in the proximity of the **NSD438** terminal phenyl ring, and hydrophobic interactions with K341 carbonyl chain were conceivable. In light of these observations, we developed F338A and K341A mutants and compared the affinity of a subset of our NN*h*AKIs analogs with the affinity toward the wt enzyme. However, besides the peculiar interactions that each enzyme residue could establish or not with **NSD438**, to localize the site of binding for our NN*h*AKIs, we decide to select, for our mutagenesis studies, some residues that border and define the hypothetical binding site. We decided to focus on the phenylmercaptomethyl subpocket, as in **NSD438**, the phenylmercaptomethyl was predicted to possess a larger surface of interaction with respect to the pyrrolobenzoxazepinone scaffold that was found perpendicularly oriented with respect to α3 helix in our previous computational studies. On the basis of the above, Q74, Q78, H107 were selected for Ala scan. A double mutant Q74A-F338A was also considered.

Thus, specific primers were designed (Table S1) to create single and double amino acid substitutions of *h*AK using site-directed PCR mutagenesis. Each mutant, expressed in *E. coli* (DH5α), purified as His_6-tag recombinant protein, once biochemically characterized *in vitro*, would have given data allowing us to validate the hypothesized inhibitor binding site.

For exploring the effect of single and double mutations on *h*AK on the inhibition potency of our NN*h*AKIs, besides our hit compound *rac*-**NSD438**, we selected a small set of analogs characterized by inhibition potencies ranging from 1.0 to 12.5 μM on the wt enzyme. All the compounds were used as racemic mixtures as computational studies already predicted no stereoselectivity of interaction for **NSD438** (16). To confirm this hypothesis, we developed a stereoselective approach for (*S*)-**NSD438** and (*R*)-**NSD438** synthesis. The outcome on *h*AK wild-type inhibition by compounds (*R*)- and (*S*)-**NSD438** was in total agreement with the computational predictions, and no difference was observed, in this study, in the inhibition potency of both enantiomers with respect to the racemic mixture of **NSD438**. In the selection process of inhibitors to be engaged in this biochemical study, structural diversity in terms of terminal aryl moiety sizes, electronic properties, and presence of H-bonding donor/acceptor groups (Table 1) were taken into account. Table 1 summarizes the structures of the selected compounds and their IC_{50} values against wt-*h*AK.

Stereoselective synthesis of compounds (S)- and (R)-NSD438

Although the racemic mixture *rac*-**NSD438** proved to be separable in the single enantiomers by HPLC analytical methodologies, the poor solubility of this compound in typical mobile phases severely limited the scalability of this method. Moreover, the oily nature of **NSD438** hampered the possibility to establish the absolute configuration by X-ray techniques. These issues prompted us to develop a straightforward stereoselective strategy to generate the single enantiomers. We already settled and proposed a suitable chemical strategy (20) which we herein exploit for the preparation of both **NSD438** enantiomers. The chemical route employed for the stereoselective synthesis of compounds (*R*)- and (*S*)-**NSD438** is reported in Scheme 1. Starting from toluene (**1**), a standard Friedel–Crafts acylation led to α-ketoacid **2** and its corresponding ethyl ester **3**. These latter were both employed for the preparation of the (+)-menthyl ester derivative **4**. Indeed, acid **2** was condensed with (+)-menthol in the presence of *p*-toluenesulfonic acid (21), while ester **3** underwent a modification of the titanium (IV) alkoxyde-catalyzed transesterification developed by Seebach (22). Accordingly, treatment of **3** with (+)-menthol in the presence of a catalytic amount of titanium isopropoxide (20 mol %) in toluene provided the corresponding (+)-menthyl ester **4** in high yield. Reaction of **4** with ethyl magnesium bromide in the presence of 2 eq of zinc chloride afforded chiral α-hydroxy ester **5** in good yield and with a 92:8 *diastereomeric ratio* (*dr*) by NMR determination (the two diastereoisomers being easily separated by flash chromatography). The ensuing conversion of menthyl ester to its corresponding methyl derivative was performed in order to overcome subsequent issues with the cleavage of menthyl ester on more hindered substrates which required harsh conditions and provided extremely poor yields. Accordingly, saponification was performed providing the corresponding acid **6** in turn converted into the methyl ester **7** by a mild procedure employing methyl iodide in the presence of potassium carbonate (23). SN_{Ar} performed on derivative **7** on the activated aryl fluoride 4-nitro-2-pyrrolylfluorobenzene provided the aryl-alkyl ether **8** in good yield. The subsequent reduction performed with tin(II) chloride in refluxing ethanol led to aniline derivative **9**. The next one-pot reaction was a diazotization–dediazotization and provided the deaminated product **10** in moderate yield. The reaction encompassed the use of sodium nitrite in the presence of acetic acid as a mild diazotization procedure and sodium bisulfite as the reducing agent (24). Finally, starting from compound **10**, the synthetic route for the achievement of the pyrrolobenzoxazepine scaffold fully traced out the racemic synthesis already reported, with alkaline hydrolysis of the methyl ester and followed by an

Table 1: IC_{50} (μM) values on recombinant *h*AK mutants. Each IC_{50} value is the mean of at least two determinations. SEM is in the range between 15 and 25%

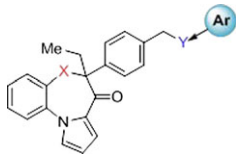

				Human AK						
Compounds	X	Y	Ar	wt	Q74A	Q78A	H107A	K341A	F338A	Q74A-F338A
NSD438	O	S		1.2	6.4	2.0	2.6	3.5	11.8	>100
14	O	S		3.5	17.4	5.9	5.1	23.2	70.2	>100
15	O	S		1.0	3.6	0.8	3.0	3.7	13.3	>100
16	O	S		2.0	10.2	1.1	6.1	4.0	30.6	>100
17	O	S		2.0	5.0	0.6	3.1	4.5	25.4	>100
18	O	O		1.2	20.3	2.3	3.3	19.8	60.5	>100
19	S	S	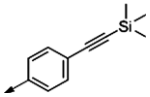	2.0	15.4	0.4	3.4	5.2	28.5	>100

intramolecular Friedel–Crafts reaction leading to the desired (*S*)-**NSD438** (25).

The chemical route for the stereoselective preparation of cyclic ketone (*R*)-**12** was already described by us (20). Starting from this optically active intermediate, a radicalic bromination and alkylation led to desired compound *(R)*-**NSD438**.

Cloning, expression, and biochemical characterization of recombinant wt-hAK and hAK mutants

Each *h*AK mutant was produced by site-directed mutagenesis based on PCR, following the method described in Methods and Materials. This approach, which allowed us to directly amplify the recombinant plasmid, utilizes two partially overlapping primers, complementary to a portion of the gene of interest, both of them bearing the desired mutation. Each primer, approximately 40 bases long, presents a superimposed region of about 20 bp, corresponding to the 5′ end of each primer, containing the specific mutation. Five pairs of primers were synthesized to replace, with alanine, the following amino acids, putatively in the inhibitor binding site: Q74, Q78, H107, K341, and F338. By removing or creating unique restriction sites, without modifying the amino acid sequence of *h*AK, we were able to distinguish mutant from the wt plasmid, used as template in the PCR. The PCR products were then treated with *Dpn*I (G^mA/TC), to fully digest the parental methylated DNA (25 restriction sites) from newly synthesized unmethylated mutant DNA. Then, 1 ng of plasmid DNA of each mutant was used to transform *E. coli* (DH5α) competent cells. Expression and purification of recombinant *h*AKs were carried out as described in Methods and Materials. The enzymes were purified from *E. coli* crude extract in a single chromatographic step using a Ni-NTA Superflow column (Qiagen). To characterize the *h*AK mutants, the enzyme was incubated in the presence of different concentrations of labeled substrate ([2,8-^{3}H]-Ado) using ATP as phosphate donor at 0.1 mM. Table 2 summarizes the kinetic parameters of recombinant *h*AK mutants compared with wt-*h*AK (16). The K_m values demonstrate that the single-site and the double-site mutations of the amino acid residues present in the novel hypothesized allosteric site of *h*AK change the enzyme affinity for the substrate, suggesting a functional relationship between the putative allosteric site and the catalytic site of the enzyme. In particular, K_{cat} and K_{cat}/K_m, which measure the enzyme turnover and the efficiency of catalysis, respectively, indicate that the introduced point mutations somehow affect the behavior of *h*AK. For instance, Q74A, Q78A, and F338A mutants have a reduced turnover (0.05, 0.05, and 0.08, respectively, compared to 0.5 of wt-*h*AK) and a 10-fold lower efficiency of phosphorylation (0.10, 0.13, and 0.10, respectively, compared to 1.25 of wt-*h*AK). As expected, the double mutant Q74A/F338A-*h*AK, although possessing a K_m slightly lower than that of wt-*h*AK, shows both a lower K_{cat} (0.02) and a lower K_{cat}/K_m (0.05), indicating a slow and inefficient phosphorylating activity. On the other hand, K341A-*h*AK displays a higher affinity for the substrate Ado (K_m: 0.17 μM) compared to wt-*h*AK, but a lower turnover (K_{cat}: 0.22); these values lead to a K_{cat}/K_m ratio similar to that reported for the wt-*h*AK. Finally, mutant H107A-*h*AK possesses a lower affinity for the substrate (K_m: 1.66 μM) and a K_{cat} similar to the wt-*h*AK, which results in a fourfold lower efficiency of phosphorylation.

It must be underlined that, from a structural point of view, although the binding clefts of Ado and **NSD438** are two distinct sites, they share a portion of the α3 helix and of the enzyme carboxylic tail. In fact, the central part of the α3 helix, from which Q74 protrudes, forms the **NSD438**

Table 2: Kinetic parameter of recombinant wt-*h*AK and mutants. K_m value is the mean of at least two determinations. K_{cat} was calculated using 46 kDa as the molecular mass of the enzyme

*h*AK	K_m (μM)	V_{max} (pmol seconds^{-1} μg^{-1})	K_{cat} (seconds^{-1})	K_{cat}/K_m (seconds^{-1}/μM)
wt	0.40 ± 0.10	10.7 ± 1.00	0.50	1.25
Q74	0.48 ± 0.20	1.05 ± 0.13	0.05	0.10
Q78	0.39 ± 0.07	1.00 ± 0.08	0.05	0.13
H107	1.66 ± 0.41	7.74 ± 0.08	0.35	0.27
K341	0.17 ± 0.02	4.86 ± 0.02	0.22	1.29
F338	0.83 ± 0.24	1.85 ± 0.12	0.08	0.10
Q74-F338	0.36 ± 0.05	0.36 ± 0.02	0.02	0.05

cleft pavement, while its end forms the Ado binding site border. Along the same lines, F338 is part of the flexible carboxylic tail, which shapes **NSD438** binding site and represents one edge of the Ado binding site. Interestingly, in the close conformation of the enzyme (PDB code: 1BX4), the flexible carboxylic tail seems to be held in place by a tight interaction (distance between the rings centroids = 4.5 Å) between F338 and W75 (this latter sitting next to Q74 on the α3 helix). Thus, we can envisage that F338A mutation, disrupting this π–π interaction, would allow a major flexibility of the carboxylic tail, not beneficial for the AK substrate affinity. Differently, the double mutant F338A-Q74A somehow regains substrate affinity showing that the two amino acids co-operate in a structural change advantageous for Ado affinity. Noteworthy, together with N68, Q67, and W75, the Q74 residue seems to be important for α3 helix positioning as its polar side chain is involved in multiple H-bonds with backbone CO and NH of P80, A84, and K82. The single mutation of Q74 does not seem to tangibly perturb the enzyme structure and conformation; however, the simultaneous mutation of Q74 and F338, which was also important in stabilizing the α3 helix position (see above), may instead allow a small shifting of the α3 helix, fruitfully affecting Ado binding. However, further studies could clarify this issue.

Inhibition assays on recombinant wt-hAK and hAK mutants and rationalization of inhibitors IC_{50} on enzyme mutants

The selected compounds, bearing differently functionalized arylmercaptomethyl moieties (Table 1), were tested on single-mutant enzymes (Q74A, Q78A, H107A, K341A, F338A) and on the double mutant (Q74A-F338A) (see Methods and Materials) to validate the proposed hypothesis of a novel allosteric binding site. The inhibition effect on *h*AKs activity was examined over a range of inhibitors' concentrations with both substrates Ado and ATP at 1 μM and 0.1 mM, respectively (Table 1). The inhibition curve for all compounds follows a sigmoid shape rather than a right Michealis Menten rectangular hyperbola. The data were fitted to the Hill equation ($r = n[A]^n/(K_d+[A]^n)$) to determine whether the inhibition exhibited cooperative characteristics. In general, our results confirm (i) a cooperative mode of action of the inhibitors, having a Hill's coefficient >1 (data not shown), and (ii) the expected reduced inhibitory activity of the compounds against *h*AK mutants (see Figure 2 for **NSD438**). The outcome on *h*AK wild-type inhibition by compounds (*R*)- and (*S*)-**NSD438** was in total agreement with the computational predictions, and no difference was observed in the inhibition potency of both enantiomers with respect to the racemic mixture (no stereoselective mode of interaction).

The previously proposed binding mode of NN*h*AKIs highlighted F338 as a key residue in the interaction with our inhibitors, as both an H-bond and a π–π interaction were found with **NSD438**. Accordingly, among all the mutations, the F338A substitution resulted as the more effective, being responsible of a substantial reduction in the inhibition potency of the compounds. Point mutations Q78A and H107A, both lining the phenylmercaptomethyl subpocket of the allosteric site, did not significantly affect the inhibition potency of the compounds if compared to the effect F338A. The other two explored mutations K341A and Q74A significantly influenced the binding of **NSD438** analogs being the Q74A mutant slightly more effective in reducing binding. Among the tested compounds, the analog **14** was the most sensible to the mutation of both K341A and Q74A. From docking calculation, it resulted that the imidazole ring occupies the same position of the mercaptophenyl group (Figure 1) and sits in proximity of both K341 and Q74. Differently from **NSD438** analogs **15**–**19**, the imidazole ring of **14** would be able to accept an H-bond from K341 or Q74 side chain, thus justifying lower inhibition potency for the K341A and Q74A enzyme mutants.

To better explore the influence of the introduced mutations on the inhibitor–enzyme interaction, we cloned and expressed a double mutant combining the single mutations which mostly affected the inhibitory activity of the compounds. Accordingly, double alanine mutant in the key residues F338 and Q74 was generated to evaluate possible additive effects in the reduction of the binding of our inhibitors. As expected from the results obtained with the single mutants, Q74A-F338A-*h*AK mutant showed a total loss of affinity for all the tested compounds (Table 1).

To further investigate whether the mutations introduced in *h*AK were only able to modulate the interaction of our inhibitors with their putative allosteric pocket, we evaluated the *h*AK inhibitory activity of 5-iodotubercidine (5-ITU), a known potent competitive inhibitor which binds the catalytic site (IC_{50} value in nM range) (19), against the most efficient mutant developed Q74A-F338A-*h*AK *in vitro*. Interestingly, like in wt-*h*AK, the double Q74A-F338A-*h*AK mutant was inhibited by 5-ITU in the nanomolar range (Figure 3), thus providing further evidence of the presence in *h*AK of an allosteric pocket independent from the catalytic/regulatory site. We definitely proved the discovery of an allosteric binding site in *h*AK for non-nucleoside inhibitors, which substantially

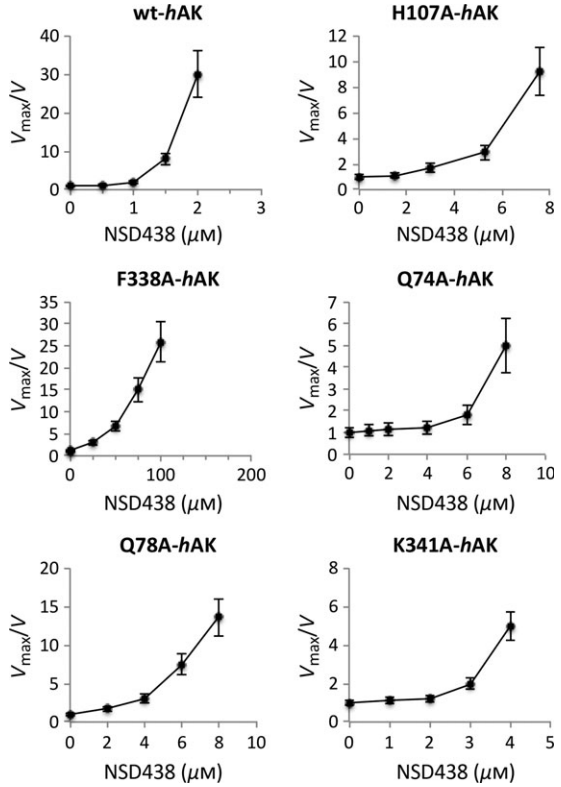

Figure 2: Effect of **NSD438** on wt-*h*AK and *h*AK mutants (each point is the average of two determinations in two independent experiments). To standardize the enzyme velocities in parallel experiments, we plotted V_{max}/V against **NSD438** concentrations. When in the assay **NSD438** concentration is 0 μM, being $V = V_{max}$, the *y*-axis value is 1. At **NSD438** increasing concentrations, being $V < V_{max}$, the *y*-axis value increases up to ∞, when $V = 0$. For the discussion about the nonlinear shape of the curve, see the text and (Ref. 16).

diverges from the same site in other enzymes of the same family.

Indeed, as stated in the introduction, AK belongs to the ribokinase family (13) of enzymes which phosphorylate the hydroxymethyl groups of a variety of sugars. Although the overall sequence identity between the members of the RK family is <30% (see Sequence Alignment in Figure S1), their tridimensional structures are indeed similar (13). Particularly, AK and ribokinase (RK) are two important ribokinase family of enzymes that share unique secondary and tertiary structural elements (13). A three-dimensional superposition of *h*AK (PDB code: 1BX4) and *h*RK (PDB code: 2FV7) demonstrates that the allosteric site identified by us highly diverges between the two proteins due to multiple mutations especially in the α3 helix and in the C-terminal tail. As for example, residues such as Q67, K71, Q74, W75 within the α3 helix of hAK are replaced in RK by A56, V60, A63, R64, respectively (see Figure S2A). Notably, the carboxylic tail of *h*AK (PDB code: 1BX4) heavily differs from that of *h*RK (PDB code: 2FV7), even in its

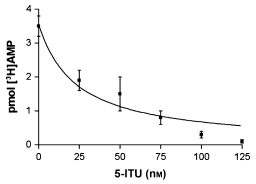

Figure 3: In vitro effect of increasing concentrations of 5-ITU on Q74AF338A-*h*AK activity (IC_{50}, 25 nM). Each point is the average of three determinations.

secondary structure, thus making impossible to unambiguously establish a clear amino acid correspondence (see Sequence Alignment in Figure S1). The same holds true when a comparison with human ketohexokinase (PDB code: 2HLZ) is performed (Figure S2B). In summary, in *h*AK, the novel allosteric site, herein identified, is definitely shaped by amino acids which are peculiar of this enzyme. To the best of our knowledge, no other ligands of RK family are known to bind this site.

Conclusion

The computational data herein discussed coupled with Ala-scan mutagenesis studies contributed to confirm the existence of a putative allosteric site on *h*AK, which is exclusively bound by our recently developed a pyrrolobenzoxa(thia)zepinone NN*h*AKIs. The discovery of an extra allosteric site into the human enzyme may be exploited for the discovery of more potent and selective NN*h*AKIs endowed with therapeutic potential.

Acknowledgments

This work was partially supported by the Consiglio Nazionale delle Ricerche/Ministro dell'Istruzione, dell'Università e della Ricerca 'Progetto d'interesse invecchiamento', and the FIRB Grant RBAU01LSR4_001 (to F.F.). L.S. was supported by a doctoral fellowship provided by Regione Lombardia, Project ID 13810040 'Plant Cell'.

Conflict of Interest

Authors declare no conflict of interest.

References

1. Pignataro G., Simon R.P., Boison D. (2007) Transgenic overexpression of adenosine kinase aggravates cell death in ischemia. J Cereb Blood Flow Metab; 27:1–5.
2. Pignataro G., Maysami S., Studer F.E., Wilz A., Simon R.P., Boison D. (2008) Downregulation of hippocampal adenosine kinase after focal ischemia as potential endogenous neuroprotective mechanism. J Cereb Blood Flow Metab;28:17–23.

3. Boison D. (2013) Adenosine kinase: exploitation for therapeutic gain. Pharmacol Rev;65:906–943.
4. Fassett J.T., Hu X., Xu X., Lu Z., Zhang P., Chen Y., Bache R.J. (2011) Adenosine kinase regulation of cardiomyocyte hypertrophy. Am J Physiol Heart Circ Physiol;300:H1722–H1732.
5. Annes J.P., Ryu J.H., Lam K., Carolan P.J., Utz K., Hollister-Lock J., Arvanites A.C., Rubin L.L., Weir G., Melton D.A. (2012) Adenosine kinase inhibition selectively promotes rodent and porcine islet beta-cell replication. Proc Natl Acad Sci USA;109:3915–3920.
6. Park J., Gupta R.S. (2013) Adenosine metabolism, adenosine kinase, and evolution. In: Masino S., Boison D., editors. Adenosine: A Key Link between Metabolism and Brain Activity. New York: Springer Science + Business Media; p. 23–54.
7. Williams-Karnesky R.L., Sandau U.S., Lusardi T.A., Lytle N.K., Farrell J.M., Pritchard E.M., Kaplan D.L., Boison D. (2013) Epigenetic changes induced by adenosine augmentation therapy prevent epileptogenesis. J Clin Invest;123:3552–3563.
8. Jia G., Fu Y., He C. (2013) Reversible RNA adenosine methylation in biological regulation. Trends Genet;29:108–115.
9. Kredich N.M., Martin D.V. Jr (1977) Role of S-adenosylhomocysteine in adenosine-mediated toxicity in cultured mouse T lymphoma cells. Cell;12:931–938.
10. Boison D., Scheurer L., Zumsteg V., Rulicke T., Litynski P., Fowler B., Brandner S., Mohler H. (2002) Neonatal hepatic steatosis by disruption of the adenosine kinase gene. Proc Natl Acad Sci USA;99:6985–6990.
11. James S.J., Melnyk S., Pogribna M., Pogribny I.P., Caudill M.A. (2002) Elevation in S-adenosylhomocysteine and DNA hypomethylation: potential epigenetic mechanism for homocysteine-related pathology. J Nutr;132:2361S–2366S.
12. Spychala J., Datta N.S., Takabayashi K., Datta M., Fox I.H., Gribbin T., Mitchell B.S. (1996) Cloning of human adenosine kinase cDNA: sequence similarity to microbial ribokinases and fructokinases. Proc Natl Acad Sci USA;93:1232–1237.
13. Park J., Gupta R.S. (2008) Adenosine kinase and ribokinase–the RK family of proteins. Cell Mol Life Sci;65:2875–2896.
14. Mathews I.I., Erion M.D., Ealick S.E. (1998) Structure of human adenosine kinase at 1.5 A resolution. Biochemistry;37:15607–15620.
15. Parducci R.E., Cabrera R., Baez M., Guixe V. (2006) Evidence for a catalytic Mg^{2+} ion and effect of phosphate on the activity of *Escherichia coli* phosphofructokinase-2: regulatory properties of a ribokinase family member. Biochemistry;45:9291–9299.
16. Butini S., Gemma S., Brindisi M., Borrelli G., Lossani A., Ponte A.M., Torti A. *et al.* (2011) Non-nucleoside inhibitors of human adenosine kinase: synthesis, molecular modeling, and biological studies. J Med Chem;54:1401–1420.
17. Liu H.T., Naismith J.H. (2008) An efficient one-step site-directed deletion, insertion, single and multiple-site plasmid mutagenesis protocol. BMC Biotechnol;8:91–100.
18. Chung C.T., Niemela S.L., Miller R.H. (1989) One-step preparation of competent *Escherichia-coli* – transformation and storage of bacterial-cells in the same solution. Proc Natl Acad Sci USA;86:2172–2175.
19. Ugarkar B.G., DaRe J.M., Kopcho J.J., Browne C.E. III, Schanzer J.M., Wiesner J.B., Erion M.D. (2000) Adenosine kinase inhibitors. 1. Synthesis, enzyme inhibition, and antiseizure activity of 5-iodotubercidin analogues. J Med Chem;43:2883–2893.
20. Brindisi M., Gemma S., Alfano G., Kshirsagar G., Novellino E., Campiani G., Butini S. (2013) A stereoselective route to 6-substituted pyrrolo-1,5-benzoxazepinones and their analogues. Tetrahedron Lett;54:5387–5390.
21. Basavaiah D., Krishna P.R. (1995) New cyclohexyl-based chiral auxiliaries – enantioselective synthesis of alpha-hydroxy acids. Tetrahedron;51:12169–12178.
22. Xiang J.M., Li B.L. (2010) The stereoselective synthesis of 2-Aryl-2-hydroxybutanoic acid via menthyl chiral auxiliaries. Helv Chim Acta;93:2015–2022.
23. Ji F., Wu W., Dai X., Mori N., Wu J., Buchwald P., Bodor N. (2005) Synthesis and pharmacological effects of new, N-substituted soft anticholinergics based on glycopyrrolate. J Pharm Pharmacol;57:1427–1435.
24. Geoffroy O.J., Morinelli T.A., Meier G.P. (2001) Chemoselective one-pot reductive deamination of aryl amines. Tetrahedron Lett;42:5367–5369.
25. Fattorusso C., Gemma S., Butini S., Huleatt P., Catalanotti B., Persico M., De Angelis M. *et al.* (2005) Specific targeting highly conserved residues in the HIV-1 reverse transcriptase primer grip region. Design, synthesis, and biological evaluation of novel, potent, and broad spectrum NNRTIs with antiviral activity. J Med Chem;48:7153–7165.

Note

[a]Glide (2009). New York, S., LLC.

Supporting Information

Additional Supporting Information may be found in the online version of this article:

Figure S1. Multiple sequence alignment of AK, Ribokinase RK and Ketohexokinase (KHK) from humans, mouse and rat.

Figure S2. Superposition of the crystal structure of *h*AK with that of *h*RK and of *h*KHK.

Appendix S1. Experimental details and characterization for the synthesized compounds.

Table S1. Primer used for site-directed mutagenesis.